Parallelization of 3-D Global FDTD Earth-Ionosphere Waveguide Models at Resolutions on the Order of ∼1 km and Higher

Alireza Samimi and Jamesina J. Simpson, *Senior Member, IEEE*

***Abstract*—Three-dimensional finite-difference time-domain (FDTD) models of the global Earth-ionosphere waveguide were first introduced in the early 2000s. These models have been applied to a wide variety of applications at ultralow and extremely low frequencies, including hypothesized earthquake precursors, Schumann resonances, and space weather hazards to electric power grids. The deployment of petascale supercomputers and future plans for exascale supercomputers introduce for the first time the possibility of generating ultrahigh-resolution FDTD models of the Earth-ionosphere waveguide at 1 km and higher globally. When including a magnetized ionospheric plasma algorithm, these models may simulate very low frequencies for the first time on a global scale and/or extend to altitudes well above 100 km as needed. We describe the parallelization strategy of efficient latitude–longitude FDTD Earth-ionosphere models and describe some example performances on the Blue Waters supercomputer, which has over 360 000 computational cores.**

***Index Terms*—Earth, extremely low frequency (ELF), finite-difference time-domain (FDTD) methods, ionosphere, magnetized plasma, propagation, sphere, ultralow frequency (ULF), very low frequency (VLF).**

I. Introduction

THREE-DIMENSIONAL finite-difference time-domain (FDTD) models [1], [2] of the global Earth-ionosphere waveguide were first introduced in the early 2000s [3]–[5] and subsequently developed and applied by other groups (e.g., [6]–[10]). The highest resolution achieved to date by any of these Earth-ionosphere models on a global scale is nominally $\sim 40 \times 40 \times 5$ km using a latitude–longitude grid-cell arrangement [4] and ∼60 km laterally using a geodesic grid-cell arrangement [5]. The resolution of ∼40 km laterally for the latitude–longitude grid was made possible via a novel adaptive cell-combining technique applied to cells in the East–West directions as either Pole is approached [4]. This technique also permitted use of a maximum time-step near the Courant limit for the larger grid cells in the vicinity of the Equator. These nominal global resolutions have in some cases been locally refined in the lateral (North–South and East–West) directions in order to better resolve regions of specific interest [10], or locally refined in the radial (vertical) direction near the Earth's surface in order to better resolve the Earth's topography and lithosphere composition [11].

Recently deployed petascale supercomputers and plans for exascale supercomputers introduce for the first time the possibility of generating ultrahigh-resolution FDTD models of the Earth-ionosphere waveguide on a global scale. Whereas previous global FDTD models to date were limited to frequencies below 500 Hz [12], petascale supercomputers permit modeling of frequencies well over an order of magnitude higher—into the very low frequency range (VLF: 3–30 kHz). Propagation modeling at VLF requires a 3-D FDTD magnetized ionospheric plasma algorithm, of which a couple versions have been applied to global FDTD models (e.g., [13] and [14]). Global modeling of VLF propagation introduces new application possibilities, such as geolocation, propagation from lightning, communications, etc. Global FDTD models of VLF propagation have the advantage over previous 2-D FDTD models (e.g., [15] and [16]) of solving for the fully 3-D wave propagation physics within magnetized ionospheric plasma (such as Faraday rotation), scatterings from objects and terrain variations in 3-D space, as well as for the wrap-around of signals (e.g., the long-propagation path signal may be of higher amplitude than the short-propagation path signal under certain circumstances). Global FDTD models also offer many advantages over previous analytical and frequency-domain solutions (e.g., the Long Wave Propagation Code and solutions by Wait and many others) [16] since FDTD can account for the Earth's complete topography, oceans, geomagnetic field, realistic disturbed ionospheric currents, and arbitrary source time waveforms (not just sinusoidal sources).

To obtain sufficient accuracy, FDTD generally requires 10 grid cells per free-space wavelength, λ_o. As such, a 1-km global grid resolution would permit modeling of frequencies up to 30 kHz (through the VLF range). However, the ionosphere shortens the propagation wavelength, and this must be accounted for when choosing a grid resolution, depending on the altitude to which the model extends, and the corresponding ionospheric parameters. We note that according to [17], the resolution in the radial/vertical direction could be as little as $7.5\lambda_o$ to somewhat ease the computational burden.

Parallelizing 3-D global latitude–longitude FDTD models at resolutions of ∼1 km and higher, however, is not straightforward. This letter presents the challenges and a solution to

Manuscript received January 23, 2016; revised February 27, 2016; accepted March 12, 2016. Date of publication March 23, 2016; date of current version December 20, 2016. This work was supported in part by Blue Waters Sustained-Petascale Computing Project Award #1440023, which was supported by the National Science Foundation (NSF) Awards OCI-0725070 and ACI-1238993 and the State of Illinois, and NSF CAREER Award 0955404.

A. Samimi was with the Department of Electrical and Computer Engineering, University of Utah, Salt Lake City, UT 84112 USA. He is now with Nanometrics, Milpitas, CA 95035 USA (e-mail: arsamimi450@gmail.com).

J. J. Simpson is with the Department of Electrical and Computer Engineering, University of Utah, Salt Lake City, UT 84112 USA (e-mail: jamesina.simpson@utah.edu).

Digital Object Identifier 10.1109/LAWP.2016.2545526

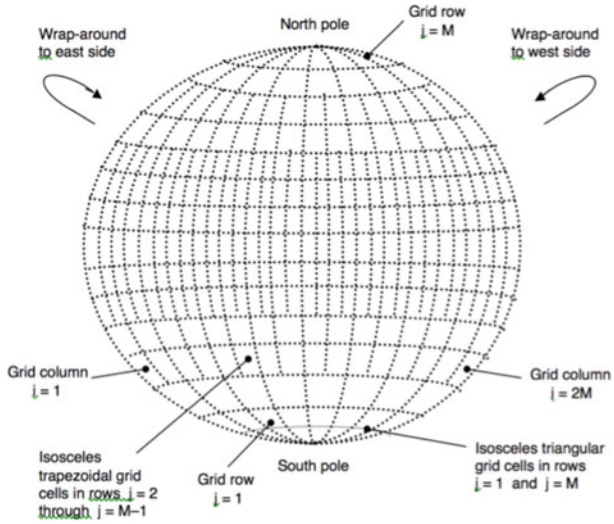

Fig. 1. Layout of the 3-D FDTD latitude–longitude grid as seen from a constant radial coordinate. Note: Not drawn to scale. Adapted from [5].

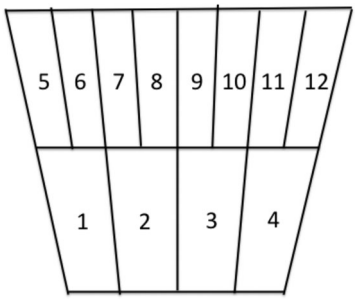

Fig. 2. Twelve example spherical grid cells extending over an East–West merging of cells in the Southern hemisphere as viewed on the Earth.

parallelizing such models (specifically the model discussed in [4]). Parallelization of cubic FDTD grids in Cartesian coordinates have previously been discussed in the literature (e.g., [18] and [19]). Thus, this letter only addresses the nuances of parallelizing the global FDTD model of [4] relative to a Cartesian grid.

We note that the parallelization of global geodesic FDTD models [20] is much more straightforward than for the latitude–longitude models discussed in this letter. However, magnetized ionospheric plasma algorithms have so far not been developed for geodesic grids, thereby limiting their applicability to frequencies below ∼1 kHz.

II. Global FDTD Model Overview

Fig. 1 illustrates a 2-D slice of the 3-D grid as seen from a constant radial coordinate. In the direction of either Pole from the Equator, at latitudes wherein the width of the cells in the East–West direction reduces to less than one half the width of the cells at the Equator, every two cells in the East–West direction are merged into one. This process may be repeated as needed, depending on the desired nominal resolution of the grid. No instabilities are introduced by the cell merging.

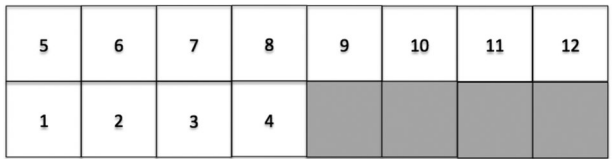

Fig. 3. Twelve numbers stored in an array corresponding to electric/magnetic field values stored in the 12 grid cells shown in Fig. 2 extending over an East–West merging of cells in the Southern hemisphere. The four dark gray values correspond to "ghost cell" numbers that take up memory but are not used in the computation.

TABLE I
Summary of the Number of Grid Cells and Maximum Time-Step Increment for a Few Example Resolutions

Nominal Lateral Resolution	#Cells in East–West Direction along Equator	#Cells in North–South Direction	Total Cells per Radial Coordinate	Maximum Δt (assuming 1-km radial resolution)
300 m × 300 m	131 072	65 536	6 698 637 136	0.37 μs
600 m × 600 m	65 536	32 768	1 674 680 144	0.73 μs
1.2 km × 1.2 km	32 768	16 384	418 649 936	1.3 μs

Table I summarizes the number of grid cells at each radial coordinate for a few example resolutions. The maximum-time step increment, Δt, is also listed for each resolution. The grid cells immediately around the Poles restrict the maximum Δt the most. Using Table I as a guide, an example 3-D global model extending from the Earth's surface to an altitude of 100 km at a resolution of 1.2 × 1.2 × 1 km would be comprised of a total of ∼41.8 billion grid cells. At ∼300 × 300 × 1000 m resolution, the grid would be comprised of ∼669 billion grid cells. For such cases wherein the model does not extend into the lithosphere, a surface impedance boundary condition may be used at the Earth's surface [2]. The Earth's topography, lithosphere composition, ionospheric content, geomagnetic fields, etc., may be populated using data from the National Geographic Data Center, the International Reference Ionosphere, etc.

III. Parallelization Strategy

The first step in parallelizing the global model is to set an upper limit on how many cells, including ghost cells (which use up memory but are not needed in the calculation), will be assigned to each processor. Figs. 2 and 3 illustrate the cause of ghost cells in the model. This upper limit will be referred to as *Max_Cells*. It is important to set this upper limit so that no one processor runs out of available memory. In our case, a short code was run separately before the FDTD simulation to set *Max_Cells* and determine the number of processors required for the simulation.

Below are summarized important considerations in distributing the cells as equally as possible in each region of the grid while limiting as much as possible the number of "ghost" cells. Next, special considerations for setting up communications between processors are discussed.

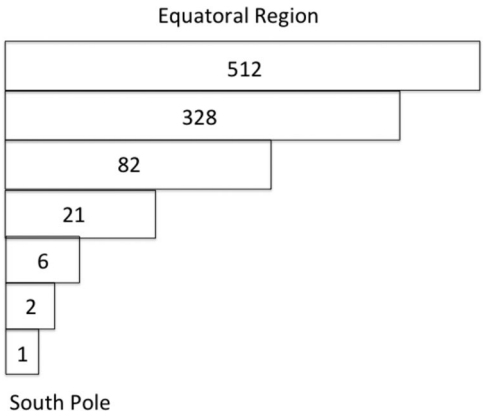

Fig. 4. Number of processors extending in the East–West direction at each row of processors between the South Pole and Equatorial Region for a ∼600 × 600 × 1000-m grid having *Max_Cells* = 163 840 cells on each processing core, assuming 10 cells in the radial direction. Note: Not drawn to scale.

A. Equatorial Region

The region near the Equator that does not include any merging of cells is the Equatorial Region. This is the most straightforward region to parallelize because it resembles a Cartesian grid (the only change being to the updating coefficients to reflect the trapezoidal shape of the cells). This region may be divided onto the available processors in a straightforward manner.

B. Polar Region

For all of the resolutions utilized to date, the number of cells in the East–West direction immediately around the Poles is exactly eight. Furthermore, merging of cells occurs most frequently near the Poles. As a result, a single core should contain the grid cells nearest each Pole and extend across the full East–West direction of the grid. For an example resolution of ∼600 × 600 × 1000 m with *Max_Cells* = 163 840, the processor at each Pole has 39 rows of grid cells in the North–South direction, and these 39 rows include five incidences of cell merging at specific latitudes.

C. Merging of Cells Region

In between the processor at the Pole and the processors in the Equatorial region is the Merging of Cells Region. In this region, the division between processors should be set slightly below (in the Southern hemisphere) or above (in the Northern hemisphere) a cell merging. Otherwise, if the division between processors is set just after a cell merging, that layer of processors will need twice as many cells in the East–West direction to accommodate the doubling of the cells, and the majority of these extra cells will be "ghost" cells. For an example resolution of ∼600 × 600 × 1000 m with *Max_Cells* = 163 840 and 10 cells in the radial direction, the division of processors is shown in Fig. 4 for the Southern hemisphere (the Northern hemisphere is a mirror image). Moving from the Pole toward the Equator, the number of processors extending in the East–West direction at each row of processors is 1 (extending to the 39th row of cells, as discussed in the "Polar Region" Section above), 2 (extending to the 79th row), 6 (extending to the 161th row), 21 (extending to the 324th row), 82 (extending to the 650th row), 328 (extending to the 1305th row), and ending with 512 in all the layers of the Equatorial region.

D. Communications Between Processors

Communications between processors in the radial direction are analogous to Cartesian FDTD models. Likewise, communications in the East–West direction are analogous to Cartesian FDTD models as well, except that special consideration must be taken in the Merging of Cell and Polar Regions to account for ghost cells (i.e., so that data are sent to the correct processor and grid cell number, especially across the periodic boundary). Likewise, communications between processors in the North–South direction in the equatorial region are analogous to Cartesian FDTD models.

The most challenging communications are in the North–South directions in the Merging of Cells and Polar Regions. For example, the processor including the South Pole must send its border data to two processors to the North. Below is an example code segment for sending Ephi components (electric fields oriented in the East–West direction or phi-direction) in the northward direction:

```
do while (send_Ephi_north(i,1) / = −1)
    j = jend_Ephi
    do ii = send_Ephi_north(i,1), send_Ephi_north(i,2)
          do r = rstart_Ephi, rend_Ephi
          Ephi_send_n(ii,r) = Ephi(ii,j,r)
     enddo
enddo
call mpi_send(Ephi_send_n(send_Ephi_north(i,1):
     send_Ephi_north(i,2),:),
send_Ephi_north(i,3),MPI_REAL,
     send_Ephi_north(i,4), tag, MPI_COMM_WORLD,
ierr)
enddo
```

where send_Ephi_north is an array that holds (at the $j = 1$ and $j = 2$ positions of the array) the start and end values, respectively, in the phi-direction of the Ephi array that must be sent to the processor to the North. Also stored (at $j = 3$) in send_Ephi_north is the number of values that will be sent, and the processor number to which the data should be sent (at $j = 4$). All of these values can be determined before time-stepping begins. The variables MPI_REAL, tag, MPI_COMM_WORLD, and ierr are standard MPI values as also used in parallelized Cartesian FDTD models. The loop increments through j-values until all of the communications required by that processor are complete (twice for the case of the processor including the South Pole).

IV. Performance Examples

The Blue Waters supercomputer was used to time some example global FDTD models running at resolutions on the order of 1 km and less and parallelized in the manner described above.

Blue Waters is currently the fastest supercomputer on a university campus. Its peak performance is more than 13 quadrillion calculations per second, and it has more than 1.5 PB of memory. Blue Waters is a Cray XE machine composed of AMD 6276 "Interlagos" processors (nominal clock speed of at least 2.3 GHz), and it has a total of 362 240 computational cores.

The model was first run using a nominal resolution of $\sim 1.2 \times 1.2 \times 1$ km. The cells along the equator were reduced by a factor of 256 ("reduction factor"), and the code was run with 10 cells in the radial direction, resulting in rectangular grid-cell sections of $128 \times 128 \times 10$ per processor at the Equator, and *Max_Cells* = 163 840 cells on all other processing cores, including ghost cells. This distribution resulted in a total of 26 336 cores in the lateral directions (East–West and North–South), with the grid divided onto 112 cores in the North–South direction between the Poles. This code ran on Blue Waters at a rate of 0.18 seconds per time-step. Note that the reduction factor must balance: 1) the number of cells per core, so that the cores do not run out of memory; 2) the number of ghost cells (which increases as the reduction factor is increased); and 3) communications (number of field values that must be shared) between cores.

Second, the 1.2×1.2-km resolution model was run using a reduction factor of 512 (still with 10 cells in the radial direction), resulting in rectangular grid-cell sections of $64 \times 64 \times 10$ per processor at the Equator, and *Max_Cells* = 40 960 on all other processing cores, including ghost cells. This resulted in a total of 104 302 cores in the lateral directions, with the grid divided onto 214 cores in the North–South direction between the Poles. This code ran at a rate of 0.11 s per time-step. As a result, a reduction factor of 512 at this resolution significantly increases the number of required cores due to the increase in ghost cells (relative to the case of the reduction factor = 256). Furthermore, the amount of communications between cores is increased relative to the number of cells per processing core, such that the rate of computation is not scaled in relation to the increase in the number of required cores. However, although a reduction factor of 512 at 1.2-km resolution is above the range of efficient scaling on cores, operating in this range may be necessary if computations are needed within a shorter (more reasonable) amount of time, depending on the application.

The model was also run using a nominal resolution of $\sim 600 \times 600 \times 1000$ m. The cells along the equator were reduced by a factor of 512 and with 10 cells in the radial direction, resulting in rectangular grid-cell sections of $128 \times 128 \times 10$ per processor at the Equator, and *Max_Cells* = 163 840 cells on all other processing cores, including ghost cells. This resulted in a total of 104 304 cores in the lateral directions, with the grid divided onto 214 cores in the North–South direction between the Poles. This code ran on Blue Waters at a rate of 0.517 s per time-step.

V. Conclusion

The advantages and challenges of parallelizing 3-D global FDTD latitude–longitude models of the Earth-ionosphere waveguide on existing petascale and future exascale supercomputers were discussed. Petascale supercomputers have created the possibility of conducting VLF propagation studies for the first time on a global scale. Exascale supercomputers will further expand the applicability of global FDTD models, either by expanding them to higher altitudes, higher resolutions (for more accuracy), and/or higher frequencies. Applications may range from communications to radar, remote sensing, and a multitude of geophysical studies, including space weather.

References

[1] K. Yee, "Numerical solution of initial boundary value problems involving Maxwell's equations in isotropic media," *IEEE Trans. Antennas Propag.*, vol. AP-14, no. 3, pp. 302–307, May 1966.

[2] A. Taflove and S. C. Hagness, *Computational Electrodynamics: The Finite-Difference Time-Domain Method*, 3rd ed. Norwood, MA, USA: Artech House, 2005.

[3] M. Hayakawa and T. Otsuyama, "FDTD analysis of ELF wave propagation in inhomogeneous subionospheric waveguide models," *ACES J.*, vol. 17, no. 3, pp. 239–244, Nov. 2002.

[4] J. J. Simpson and A. Taflove, "Two-dimensional FDTD model of antipodal ELF propagation and Schumann resonance of the Earth," *IEEE Antennas Wireless Propag. Lett.*, vol. 1, pp. 53–56, 2002.

[5] J. J. Simpson and A. Taflove, "Three-dimensional FDTD modeling of impulsive ELF antipodal propagation and Schumann resonance of the Earth-sphere," *IEEE Trans. Antennas Propag.*, vol. 52, no. 2, pp. 443–451, Feb. 2004.

[6] H. Yang, V. P. Pasko, and Y. Yair, "Three-dimensional finite difference time domain modeling of Schumann resonance parameters on Titan, Venus, and Mars," *Radio Sci.*, vol. 1, no. 2, 2006, Art. no. RS2S03, doi: 10.1029/2005RS003431.

[7] D. L. Paul and C. J. Railton, "Spherical ADI FDTD Method with application to propagation in the earth-ionosphere cavity," *IEEE Trans. Antennas Propag.*, vol. 60, no. 1, pp. 310–317, Jan. 2012.

[8] Y. Wang and Q. Cao, "Analysis of seismic electromagnetic phenomena using the FDTD method," *IEEE Trans. Antennas Propag.*, vol. 59, no. 11, pp. 4171–4180, Nov. 2011.

[9] A. Soriano *et al.*, "Finite difference time domain simulation of the Earth-ionosphere resonant cavity: Schumann resonances," *IEEE Trans. Antennas Propag.*, vol. 53, no. 4, pp. 1535–1541, Apr. 2005.

[10] H. Xia, Y. Wang, and Q. Cao, "Local high-resolution technique in FDTD modeling of ELF propagation in the Earth-ionosphere cavity," *IEEE Antennas Wireless Propag. Lett.*, vol. 9, pp. 649–652, 2010.

[11] J. J. Simpson and A. Taflove, "A novel ELF radar for major oil deposits," *IEEE Geosci. Remote Sens. Lett.*, vol. 3, no. 1, pp. 36–39, Jan. 2006.

[12] J. J. Simpson, "Current and future applications of 3-D global Earth-ionosphere models based on the full-vector Maxwell's equations FDTD method," *Surveys Geophys.*, vol. 30, no. 2, pp. 105–130, 2009.

[13] Y. Yu, J. Niu, and J. J. Simpson, "A 3-D global Earth-ionosphere FDTD model including an anisotropic magnetized plasma ionosphere," *IEEE Trans. Antennas Propag.*, vol. 60, no. 7, pp. 3246–3256, Jul. 2012.

[14] A. Samimi and J. J. Simpson, "An efficient 3-D FDTD model of electromagnetic wave propagation in magnetized plasma," *IEEE Trans. Antennas Propag.*, vol. 63, no. 1, pp. 269–279, Jan. 2015.

[15] M. Thevenot, J.-P. Bérenger, T. Monedière, and F. Jecko, "A FDTD scheme for the computation of VLF-LF propagation in the anisotropic earth-ionosphere waveguide," *Ann. Telecommun.*, vol. 54, nos. 5/6, pp. 297–310, 1999.

[16] S. A. Cummer, "Modeling electromagnetic propagation in the Earth-ionosphere waveguide," *IEEE Trans. Antennas Propag.*, vol. 48, no. 9, pp. 1420–1429, Sep. 2000.

[17] J. P. Berenger, "FDTD computation of VLF-LF propagation in the Earth-ionosphere waveguide," *Ann. Telecommun.*, vol. 57, nos. 11/12, pp. 1059–1090, 2002.

[18] C. Guiffaut and K. Mahdjoubi, "A parallel FDTD algorithm using the MP library," *IEEE Antennas Propag. Mag.*, vol. 43, no. 2, pp. 94–103, Apr. 2001.

[19] V. Varadarajan and R. Mittra, "Finite-difference time-domain (FDTD) analysis using distributed computing," *IEEE Trans. Microw. Guided Wave Lett.*, vol. 4, no. 5, pp. 144–145, May 1994.

[20] J. J. Simpson, R. P. Heikes, and A. Taflove, "FDTD modeling of a novel ELF radar for major oil deposits using a three-dimensional geodesic grid of the Earth-ionosphere waveguide," *IEEE Trans. Antennas Propag.*, vol. 54, no. 6, pp. 1734–1741, Jun. 2006.